Hydro-epidemiological modelling of bacterial transport and decay in nearshore coastal waters

Jonathan King[1, 2], Reza Ahmadian[1, *], and Roger A. Falconer[1]

[1] Hydro-environmental Research Centre (HRC), School of Engineering, Cardiff University, Cardiff, CF24 3AA, UK

[2] JBA Consulting, 1 Broughton Park, Old Lane North, Broughton, Skipton, North Yorkshire, BD23 3FD

* Corresponding author. E-mail address: AhmadianR@cardiff.ac.uk (R. Ahmadian)

Abstract

In recent years, society has become more aware and concerned with the environmental and human health impacts of population growth and urbanisation. In response, a number of legislative measures have been introduced within Europe (and globally), which have sparked much cross-disciplinary research aimed at predicting and quantifying these impacts, and suggesting mitigation measures.

In response to such measures this paper is focused on improving current understanding of, and simulating water quality, in the form of bacterial transport and decay, in the aquatic environment and particularly in macro-tidal environments. A number of 2D and 3D hydro-epidemiological models were developed using the TELEMAC suite to predict faecal bacterial levels for a data rich pilot site, namely Swansea Bay, located in the south west of the UK, where more than 7,000 FIO samples were taken and analysed over a two year period.

A comparison of 2D and 3D modelling approaches highlights the importance of accurately representing source momentum terms in hydro-epidemiological models. Improvements in 2D model bacterial concentration predictions were achieved by the application of a novel method for

representing beach sources within the nearshore zone of a macro-tidal environment. In addition, the use of a depth-varying decay rate was found to enhance the prediction of Faecal Indicator Organism concentrations in 3D models. Recommendations are made for the use of these novel approaches in future modelling studies.

Keywords: Faecal Indicator Organisms (FIOs), bathing water quality, T90, decay rate, revised EU Bathing Water Directive

1 Introduction

The health of nearshore coastal waters is a topic of great concern globally. As a result of population growth and industrialisation, the number of polluted discharges into water bodies has increased during the 20th and 21st centuries, with much detriment to the aquatic environment. Such contamination has far reaching consequences, which include: human health impacts through recreational activity (Weiskerger and Phanikumar, 2020) and the consumption of polluted food in the form of shellfish, reduced tourism, and economic losses (DeFlorio-Barker et al. 2018; Bussi et al. 2017; Given et al. 2006).

For example, domestic and international visitors to the coast contributed $6 billion to the UK economy in 2017 (BBC, 2017; Visit Britain, 2017). In a recent study, the Scottish Government (2018) predicted a loss of $3 million per year should bathing water quality not be maintained at an acceptable level at popular beaches. Another financial incentive is the healthcare savings associated with reduced exposure of beach goers to contaminated water (Given et al., 2006). For example, DeFlorio-Barker et al. (2018) estimated that recreational waterborne illnesses cost the US economy $2.2 to $3.7 billion every year. It is therefore important to address these issues by determining the primary sources of pollution at any one location, developing an understanding of the mechanisms which lead to adverse water quality, beach closure, and implementing mitigation strategies.

To ensure protecting human health as highlighted above, legislative measures have been introduced with regard to bathing water quality. The existing legislation applicable in the EU is the revised Bathing Waters Directive (rBWD) (European Parliament, 2006) which ensures the monitoring of water quality and defines acceptable standards, based on human health risk and following guidelines released by the World Health Organisation on safe standards for recreational waters (World Health Organization, 2003). The revised Bathing Waters Directive was introduced by the European Parliament in 2007 requiring Member States to ensure all bathing waters were of 'sufficient' quality by the close of the 2015 bathing season (European Parliament, 2006). Compliance criteria are based on the monitored concentration of two Faecal Indicator Organisms (FIOs); *Intestinal enterococci* and *Escherichia coli (E. coli)* in colony forming units per 100ml (cfu/100ml). The directive requires the concentration of these organisms to be monitored over consecutive bathing seasons (May to September), in accordance with a sampling calendar. Based on the Directive 2006/7/EC of the European Parliament, samples showing abnormally elevated concentrations, caused as a result of short-term pollution incidents, or contamination attributable to a cause, expected to last less than 72 hours, such as high level of pollution following a heavy rainfall may be disregarded and retaken (European Environment Agency, 2005). Efforts must also be made to reduce the risk of bather exposure to contaminants in addition to providing regular information on bathing water quality. Therefore, the directive requires the public to be made aware of short-term pollution incidences in advance, in order for these events to be disregarded, thereby making public health a key driver for prediction.

Due to the time lag between the collection and assessment of individual samples, monitoring in this manner is not a practical way of providing rapid public feedback to prevent exposure (Feng et al., 2015). To enable accurate and fast dissemination of information it is therefore in the interest of the governing authority to develop predictive tools to provide water quality forecasts and warning systems (Bedri et al., 2014, 2016; Chen and Liu, 2017; DHI, 2017a, b; Weiskerger and Phanikumar, 2020). Not only would this comply with the rBWD but it could enable the

identification, reduction and removal of major pollution sources, increasing the likelihood of a bathing water being assigned Blue Flag status (Bedri et al., 2015; Lea, 1996).

There are two main approaches to the development of predictive tools to provide water quality forecasts and warning systems: data driven modelling based on extensive field measurements, and process-based hydro-epidemiological models. Herein the latter approach is used, with the aim being to improve our understanding of fundamental processes affecting the fate and transport of bacterial pollution, in order to enhance the management of bacterial sources, development of predictive tools, and assessing beach monitoring and management practices.

This study examines and investigates the use of two novel techniques, as well as the methods which have been used to date for the prediction of bacterial decay in 2D and 3D model frameworks, using a data rich macro-tidal bay as a study site.

2 Methodology

2.1 Study Site

Swansea Bay is situated on the north shoreline of the Bristol Channel, located in the south west of the UK, and is a popular location among tourists and the local community (see Figure 1). The Bay contains two bathing water sites: Swansea Bay and Aberafan, both of which received a 'good' rating in the most recent bathing water assessment period. Swansea Bay was chosen for this study due to the tidal nature of the Bay, the number of FIO point sources and, more importantly, a large quantity of measured FIO data, where more than 7,000 FIO samples were taken and analysed over a two-year period.

The Bay is subject to 85 different inputs (see Figure 1b) including three main rivers discharging into the Bay: The River Tawe, River Neath and River Afan. There is a semi submerged barrage located on the River Tawe, which only overtops at tides over 3.05 m above Ordinance Datum. However, the River Neath and River Afan are tidal up to about 10 km and 1 km upstream from

the coast, respectively. Primary surface water and sewage discharges were recorded at 15-minute intervals over the 2011 bathing season (May - September) and October - November 2012 for the Smart Coasts project (Aberystwyth University and University College Dublin, 2018) as shown in Figure 1c, although data were unavailable for Combined Sewer Overflow (CSO) spills. The rBWD requires samples to be taken at a minimum depth of 0.5 m (Bedri et al., 2016; Bomminayuni, 2015) at the Designated Sampling Point (DSP) for each bathing water site. However, the tidal range in the Bay exceeds 10 m and the tidal flats are exposed up to a distance of 1500 m from shore during high spring tides. This prevents readings being taken at each bathing water site at only one location for the rBWD. Therefore, the water quality at Swansea Bay and Aberafan were monitored along BW1 and BW2 transects respectively as shown in Figure 1c. Figure 1c also depicts the locations of offshore sampling points used for model validation and calibration. The variability in the sampling location is shown in Figure 2 which presents the sampling points along BW1, recorded throughout the 2011 bathing season at 30-minute intervals from 07:00 to 16:00.

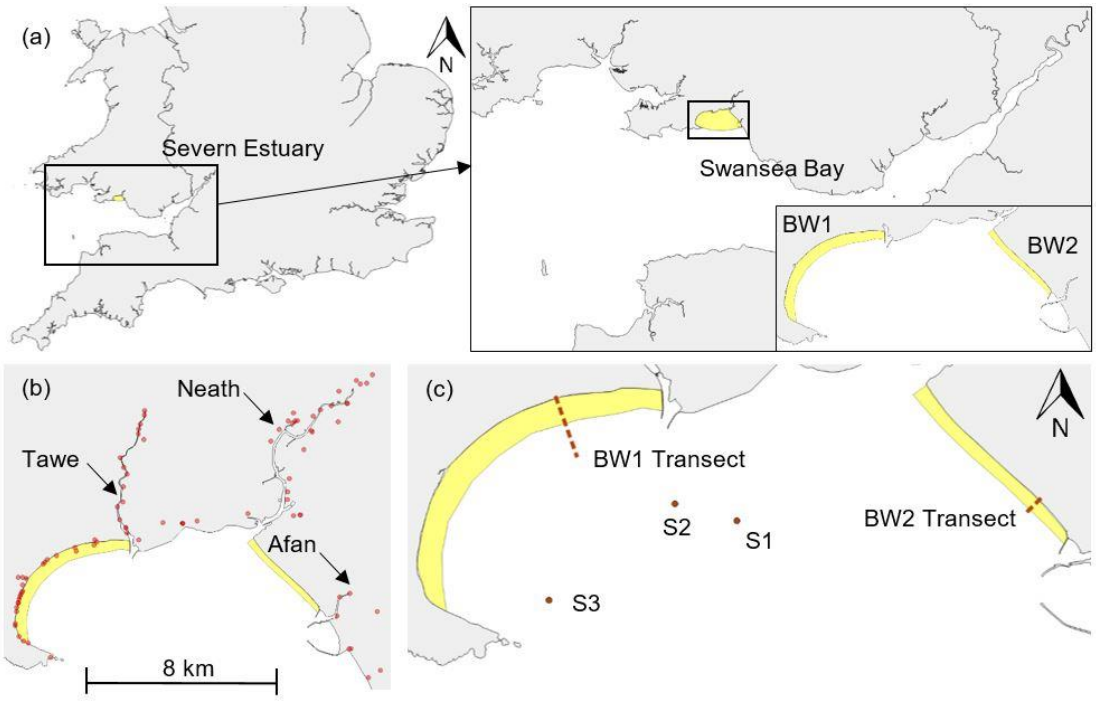

Figure 1: (a) Location of bathing waters within Swansea Bay, Severn Estuary, UK: BW1 - Swansea Bay, BW2 – Aberafan (b) Location of FIO inputs (c) Location of transects (dashed lines) and offshore monitoring points (dots)

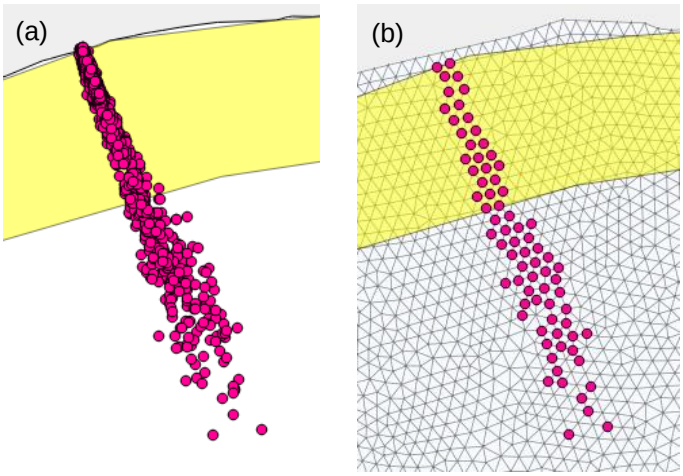

Figure 2: FIO sampling locations throughout the 2011 bathing season (a) [Aberystwyth University and University College Dublin, 2018], and the respective 2D mesh nodes (b)

2.2 Hydrodynamic models

The open-source models TELEMAC-2D and TELEMAC-3D (Galland et al., 1991) were chosen for this study to compliment previous research applications in the field of hydro-epidemiological

129 engineering (Abu Bakar et al., 2017a, Bedri et al., 2013; Kopmann and Markofsky, 2000).
130 Developed by Electricité de France, the models solve the Navier-Stokes Equations over an
131 unstructured finite element grid (Hervouet, 2007). Further details are provided in the next
132 section.
133
134 Two computational meshes of the Bristol Channel and Swansea Bay were created, one each for the
135 2D and 3D models. The 3D domain comprised a 2D mesh repeated over 5 uniformly distributed
136 sigma layers and extends over the same area apart from the rivers in Swansea Bay, as shown in
137 Figure 3. To remove the need for coupling with a 1D model, the 2D model was extended up the
138 River Tawe and to the tidal limits of the rivers Afan and Neath. However, these reaches were
139 excluded from the 3D model to reduce the computational time and unnecessary vertical
140 refinement in regions where 3D effects were of limited concern. Note that at the time of writing,
141 coupling between the latest release of TELEMAC-3D (v7p3r2), and the 1D river model TELEMAC-
142 MASCARET, was not possible.

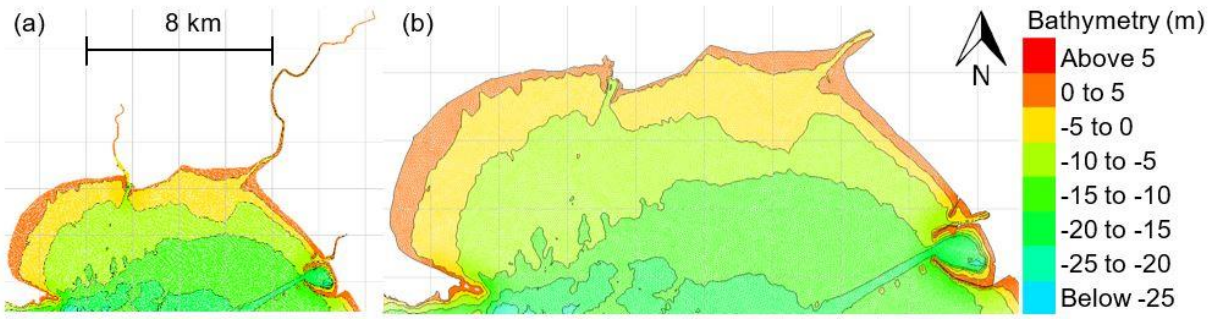

143

144 *Figure 3: Extent of 2D (a) and 3D (b) unstructured computational meshes of Swansea Bay.*
145 *Bathymetry relative to mean sea level (MSL)*

146 Bacterial sources were included as a concentration (cfu/100 ml) time series. Source locations
147 within each domain are shown in Figures 4 and 5, respectively. In the 3D model, the bacterial
148 source inputs distributed within each reach were combined into a single source point, whereas
149 those in the 2D model retained their true position.

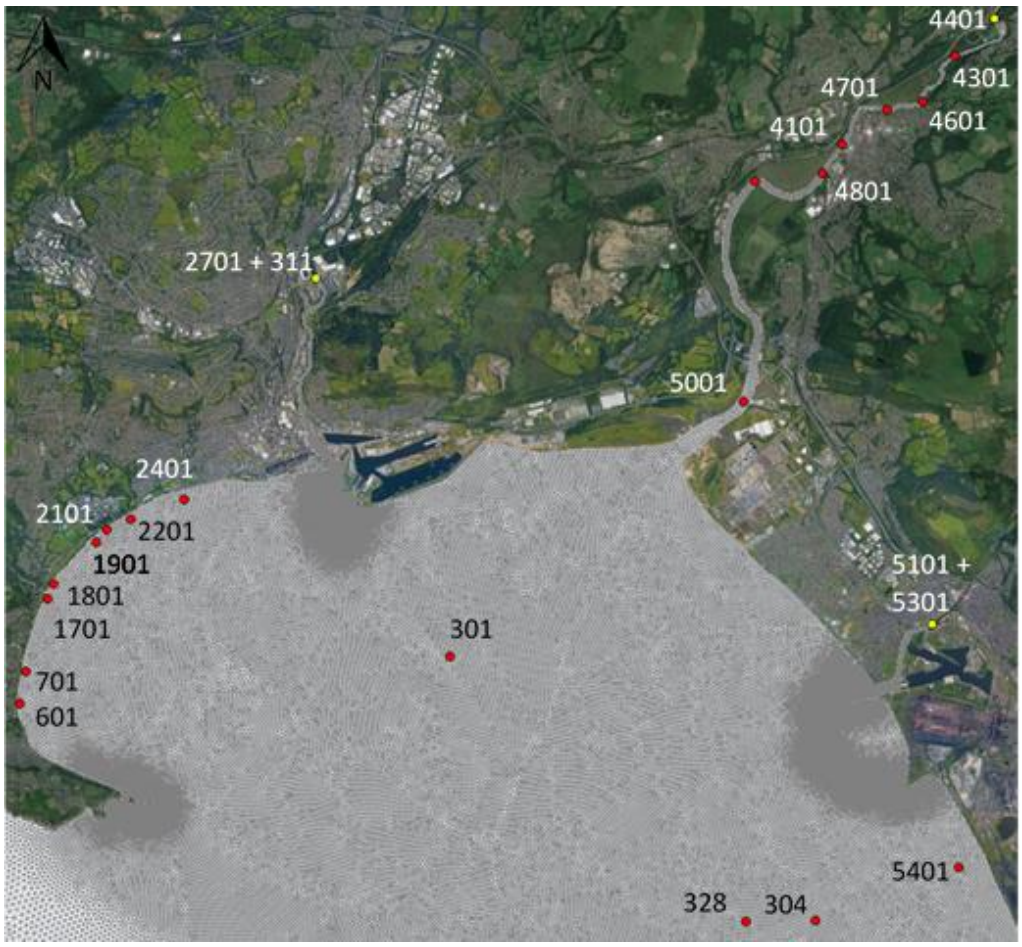

Figure 4: Primary input locations of bacterial sources within the 2D model domain of Swansea Bay – year 2012; point sources (red dots) and boundary conditions (yellow dots) with the relative ID No.

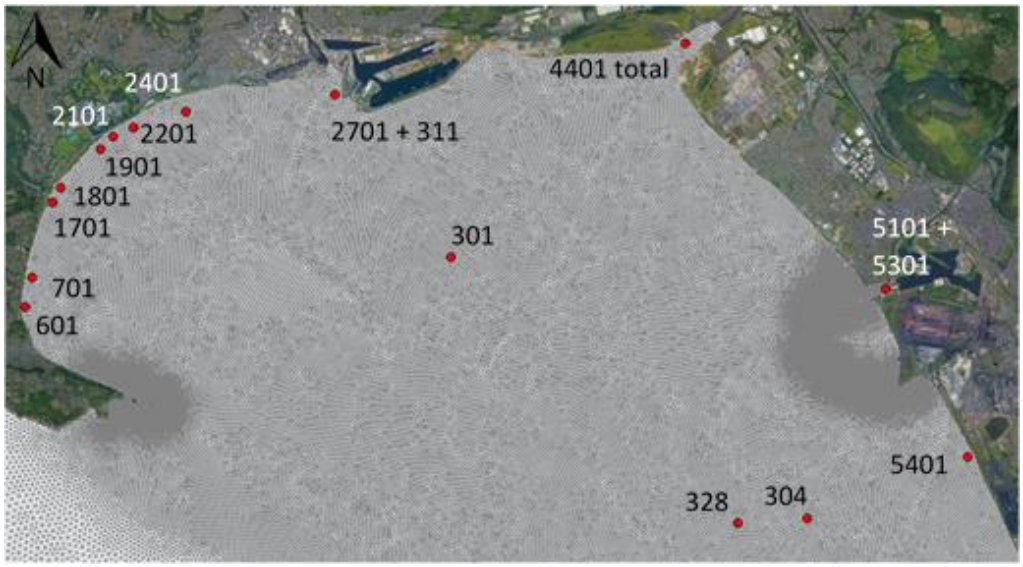

Figure 5: Primary input locations of bacterial sources within the 3D domain – year 2012; point sources (red dots) with the relative ID No.

Both meshes extend from the River Severn tidal limit close to Gloucester to the outer Bristol Channel close to Lundy Island, as shown in Figure 6, in order to capture the hydrodynamics of the Severn Estuary and Bristol Channel as has been widely used in previous studies (Ahmadian et al, 2014, Coz et al., 2019 and Guo et al., 2020). Bathymetry data was obtained from EDINA Digimap, relative to chart datum (CD), at a 30 m grid resolution (The University of Edinburgh, 2016a, b). An open boundary with a tidal water level series is imposed along the westward edge of the domain where the Bristol Channel meets the Celtic Sea.

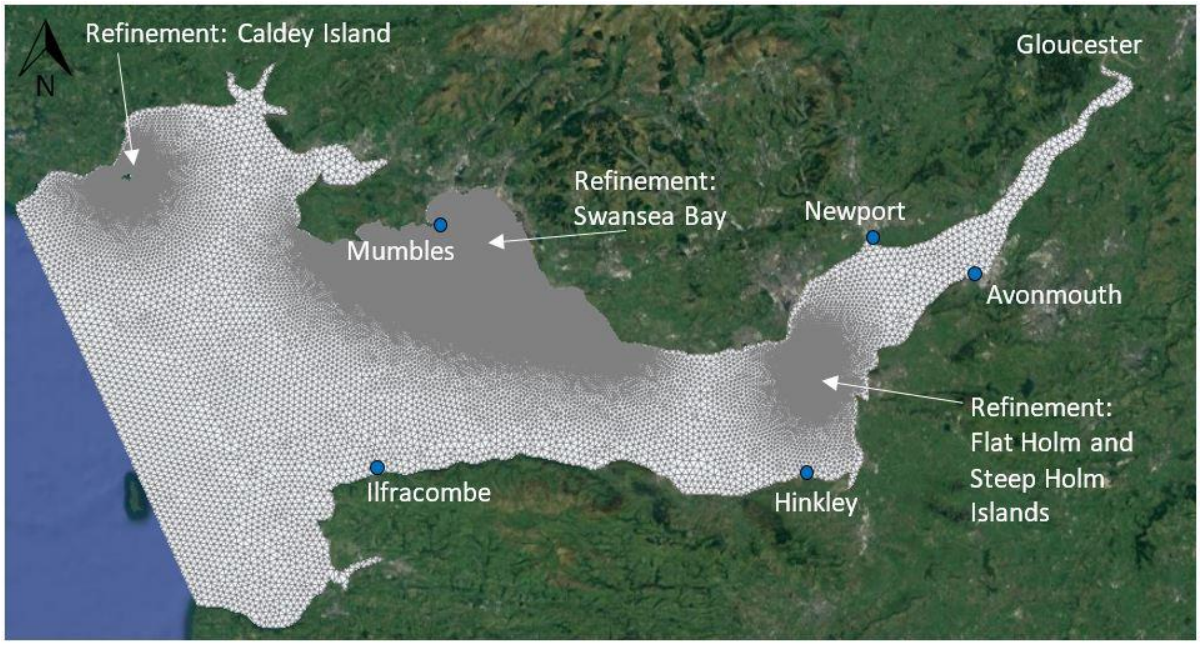

Figure 6: Extent of the unstructured computational mesh within the Bristol Channel and Severn Estuary, showing the water level monitoring locations (blue dots)

Stapleton et al. (2007a) found that a coarse grid (600 m by 600 m), was incapable of capturing localised features, such as pollutant plume shapes. The minimum grid size in the bay was limited to 30 m to capture bathymetric features as closely as possible. Therefore, the mesh size in Swansea Bay was determined based on sensitivity analysis of the different meshes. Two computational meshes were developed; using a 25 m and 50 m mesh in Swansea Bay, and increasing at a uniform rate of 1.2 to 1,000 m in the outer Bristol Channel and the Severn Estuary. From the grid dependence model tests the model results were found to be insensitive to the mesh size for the grid resolutions studies and a 50 m grid size was therefore used within Swansea Bay to increase computational efficiency. Further refinements of the grid size to 10m were used at various locations within the Bay to capture shoreline complexities. The 2D mesh contained 142,533 nodes and 281,440 elements, the 3D mesh contained 133,341 nodes and 264,237 elements, repeated over 5 sigma layers giving 666,705 nodes and 1,059,648 elements in total. As for similar studies the Smagorinski turbulence closure model was used in the horizontal (Bedri et al., 2015, 2013, Abu Bakar et al., 2017b, Guo et al., 2020) and vertical directions.

2.3 Fate and transport of bacteria: governing equations

Bacteria was simulated in TELEMAC as a non-conservative passive numerical tracer, represented by the advection-diffusion equation. Herein this is referred to as the tracer equation, written in 3D as shown in Equation 1 (Hervouet, 2007):

$$\frac{\partial C}{\partial t} + U\frac{\partial C}{\partial x} + V\frac{\partial C}{\partial y} + W\frac{\partial C}{\partial z} = \frac{\partial}{\partial x}\left(\nu_T \frac{\partial C}{\partial x}\right) + \frac{\partial}{\partial y}\left(\nu_T \frac{\partial C}{\partial y}\right) + \frac{\partial}{\partial z}\left(\nu_T \frac{\partial C}{\partial z}\right) + S_C \quad (1)$$

where C is the tracer concentration (units depend on the tracer but for bacteria it is cfu/100ml), t is time (s), h is the water depth (m), U, V and W are layer averaged velocities (m/s) in the x, y and z directions respectively, ν_T is the diffusion coefficient (m/s^2). S_C is the source or sink term, including both explicit and implicit terms. Bacterial decay is governed by the first order decay rate k which is commonly written as shown in Equation 2 (Chapra, 1997; Thomann and Mueller, 1987).

$$\frac{\partial C}{\partial t} = -kC \quad (2)$$

The decay rate k (1/d) is transposed into a T_{90} value, i.e. the time required for the concentration to reduce by 90% (Guillaud et al., 1997), as shown in Equation 3. This is traditionally required as a user input value in TELEMAC and many other models.

$$T90 = \frac{2.303}{k} \quad (3)$$

Multiple methods exist to determine the T_{90} value, and which have been applied in a number of studies (Chapra, 1997; Droste, 1997; Mancini, 1978; Stapleton et al., 2007a; Ahmadian et al., 2010; de Brauwere et al., 2011; Bedri et al., 2013; Boye et al., 2015; Huang et al., 2015; Abu Bakar et al., 2017b). Two methods have been implemented in this paper: a pre-defined constant decay rate, and that proposed by Stapeleton et al (2007a). The widely used approach proposed by Mancini (1978) was also used within the study but is not described herein due to its exclusion of sediment effects and the inclusion of non-site-specific data. For further information, see King (2019).

Stapleton et al. (2007a) carried out a study on water samples taken from the Bristol Channel and Severn Estuary to determine the impact of light intensity and turbidity on bacterial decay. As a result of laboratory experiments, the T_{90} decay rate for Enterococci was found to follow Equations 4 to 8:

$$T_{90} = T_{90_2} + \left(T_{90_1} - T_{90_{*1}}\right) \quad 4$$

$$T_{90_1} = \frac{ln10}{K_B * 60 * I} \quad 5$$

$$T_{90_{*1}} = \frac{ln10}{K_B * 60 * I^{exp}} \quad 6$$

$$LogT_{90_2} = (0.0047 * Turbidity) + 0.677 \quad 7$$

$$Turbidity = 139.479 * Log(SS) - 244.736 \pm 32.678 \quad 8$$

where I is the sunlight intensity (W/m^2), I^{exp} is the fixed irradiance for the experiments (26,014 W/m^2), T_{90*1} is the sunlight dependent Enterococci mortality rate, T_{901} is the *Enterococci* mortality rate obtained from laboratory experiments, T_{902} is the turbidity related *Enterococci* mortality rate and $K_B = 1.1\times10^{-5}$ and SS is the suspended sediment concentration (mg/l). While Stapleton et al. (2007a) only investigated the decay of *Enterococci*, the value for *E. coli* can be calculated using an appropriate magnitude of K_B ($K_B = 1.3\times10^{-5}$) (Alkan et al. 1995).

2.4 Model refinements

2.4.1 Depth-varying decay rate

Bedri et al. (2013) published the first attempt at including a spatially and temporally variant decay rate within TELEMAC-3D, using the decay formula proposed by Mancini (1978), but neglected the ability of a 3D model to incorporate light attenuation throughout the water column. The decay rate was calculated using Equations 9 and 10 (Bedri et al., 2013):

$$k_i = \alpha \bar{I} \qquad 9$$

$$\bar{I} = \frac{I_a}{k_e H}\left(1 - e^{-k_e H}\right) \qquad 10$$

where H is the water depth (m), I_α is the average daily light intensity (langleys/h), $\bar{I}$ is the depth averaged light intensity, αs a proportionality constant and k_e is the light attenuation coefficient (1/m). Equation 10 is an integration of the Beer-Lambert law which, over the fully mixed water depth (Xu et al., 2002; Chapra, 1997), can be expressed as:

$$I(z) = I_0 e^{-k_e H} \quad (11)$$

where I_0 is the surface light intensity. The light attenuation coefficient k_e (1/m) may be calculated using (Chapra, 1997):

$$k_e = 0.55\, SS \quad (12)$$

where SS is the suspended solids concentration (mg/l). For a finite element model, such as TELEMAC, the governing equations are solved at each node and Equation 11 can be used without integration, such that the irradiance induced decay rate at depth is given by Equation 13 (Chapra, 1997):

$$k_i(z) = \alpha I(z) \quad (13)$$

where the light penetration at depth is given as a function of z, i.e. $I(z)$, and where this function is calculated using the Beer-Lambert law (see Equation 11). Experimental studies have confirmed this reduction in the decay rate at increasing depths below the water surface (Mattioli et al., 2017).

For completeness and to assist future studies a comparison is made with the application of Equation 11 in a finite volume model: the average light penetrating over each layer would be used. This can be calculated using the layer averaged Beer-Lambert law and using the mean value theorem for integrals:

$$\bar{I}_{layer} = \frac{\alpha I_0}{k_e\left(z_{bottom} - z_{top}\right)}\left(e^{-k_e z_{top}} - e^{-k_e z_{bottom}}\right) \quad (14)$$

where z_{bottom} and z_{top}, are the elevations at the bottom and top of the horizontal layer respectively. Figure 7 presents depth-irradiance curves calculated using Equations 10, 11 and 14. Equations 11 and 14 exhibit a comparable reduction in light intensity with depth, whereas the rate of reduction is less when using Equation 10 (i.e. a depth averaged representation). Since TELEMAC is a finite element model, Equation 11 was used in this study.

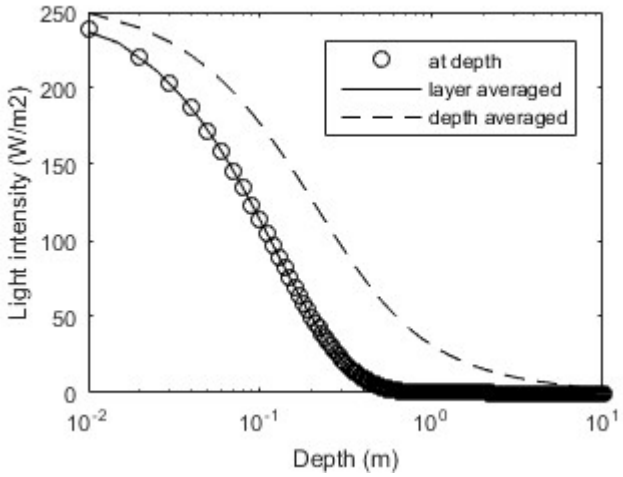

Figure 7: Comparison between irradiance at depth, calculated using: Equations 10 (depth averaged), 11 (at depth), 14 (layer averaged) and k_e calculated using Equation 12 where SS = 84.82 mg/l

2.4.2 Representation of beach sources

In modelling studies to date, bacterial sources such as CSOs and outfalls have been represented at a single point source within numerical models. However, when the grid size is too coarse, a source is distributed over a disproportionately large area and the local bathymetric features, such as that shown in Figure 8, are not captured accurately.

Furthermore, in models such as TELEMAC, where the minimum permissible water depth is 0 m, when these sources are released within shallow gradient regions the contaminated water spreads over a large area in a thin film, as shown in Figure 9 (i.e. of depth less than 1 cm, up to 1×10^{-5} m). For further details see King (2019).

Figure 8: Stream track of beach source, South Wales, UK

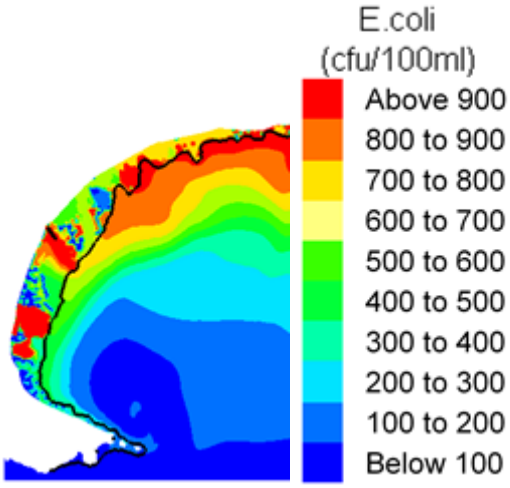

Figure 9: Depth averaged E.coli concentration in Swansea Bay at mid-tide; black line indicates a depth of 0.05m (i.e. the waterline)

While inaccurate, this is necessary to ensure mass conservation. In reality, these inputs form small streams in the beach sand (as illustrated in Figure 8), which run from the source point to the tide line. These streams can run for up to a kilometre, from the sea defence wall to the tide line, at low spring tide for this case study site. The major streams at Swansea Bay were tracked by staff at Natural Resources Wales and Swansea City Council for this research study and as a part of Smart

Coast project (Aberystwyth University and University College Dublin, 2018). The path of these streams can be seen in Figure 10.

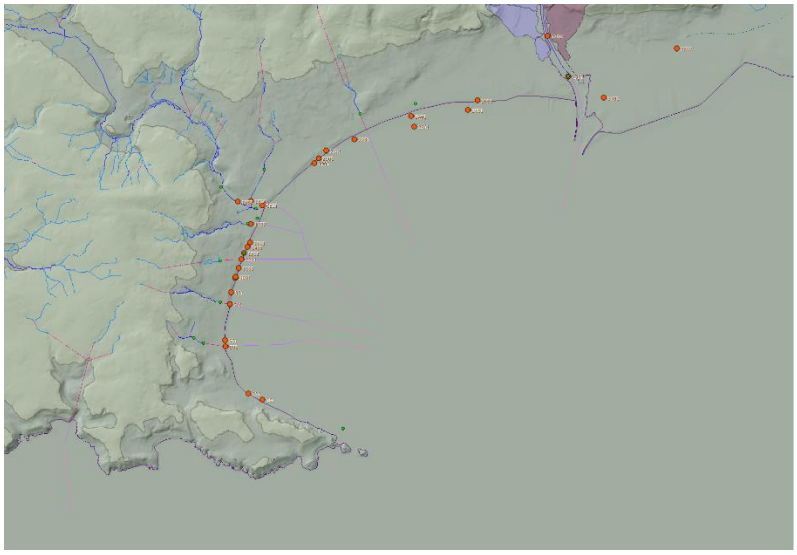

Figure 10: Stream tracks of beach sources along Swansea Bay; purple lines and red dots respectively (Aberystwyth University and University College Dublin, 2018)

From Figure 10 it is clear that including sources at high water will not represent what happens in the field and will cause inaccuracy in the predictions. The method proposed herein implements a mobile source point which tracks the waterfront along the stream path and activates releases based on the depth field. To achieve this, each source point is treated as a transect running from the sea wall to the low water line based on the field tracking of that stream. Each transect is represented by multiple source points, which discharge the same volume of water and concentration of bacteria. The source release location is changeable to ensure release is always at a point below the water line, mimicking transport within a stream. To ensure mass conservation, modifications to the TELEMAC source code only permit one point to discharge per time step, i.e. that which is closest to, and below, the waterline. Figure 11 shows the multiple source points which were used along the transects for Swansea Bay. Up to 10 source points were selected on each transect in this study as can be seen in the figure. However, more source points can be considered if the path of the streams are more complicated.

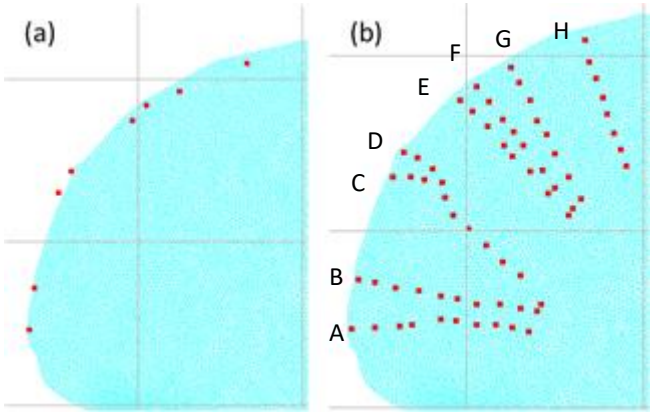

Figure 11: Static source points at the outlet location and respective source transects along Swansea Bay beach; (a) and (b) respectively

An illustration of this source representation for release at four different tidal phases is shown in Figure 12a to d. It can be seen as the tide recedes the 0.05 m depth threshold is activated at different source points along the transect (black dot). The source points along each transect were processed by multiple CPUs in parallel and the code was modified to implement this. Further information on the implementation of this method when using parallel computing methods can be found in King (2019). A similar approach was used by Feng et al. (2015), who developed a microbial transport model accounting for loading from beach sand and storm water run-off at a beach in Florida, U.S. However, the model was reduced to a 1D case for a single lumped source, and solved using the finite difference method. The grid followed a transect perpendicular to the straight uniform shoreline, which was assumed to be representative of the beach.

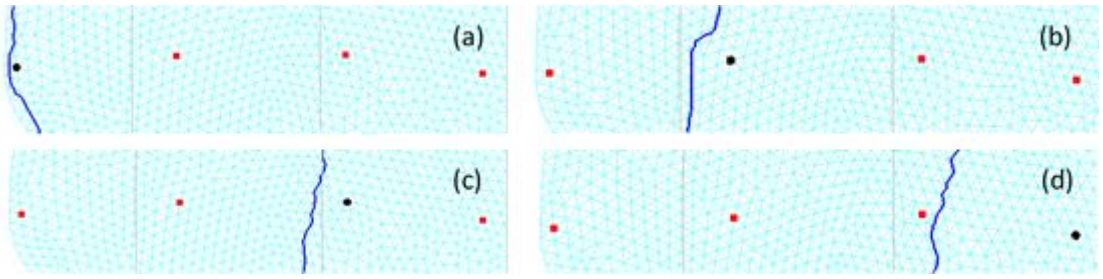

Figure 12: Illustration of improved source representation at four different tidal phases for transect A in Figure 11; blue line = threshold depth (0.05 m) which retreats seaward (right) from figure a to d, red squares = transect points, black circle

2.4.3 Parameter selection

Swansea Bay is well mixed (Ahmadian et al., 2013) with variations in temperature and salinity being shown in Figure 13. As variations through the water column are negligible they were not considered herein. Typically, in such environments a 2D modelling approach would be adopted, thus making it an ideal environment to study the difference between using depth-averaged and depth-varying approaches to calculate bacterial decay due to light intensity. Water temperature and salinity were set at 15˚C and 32 ppt respectively to match values used in previous studies (Aberystwyth University and University College Dublin, 2018; White et al., 2014).

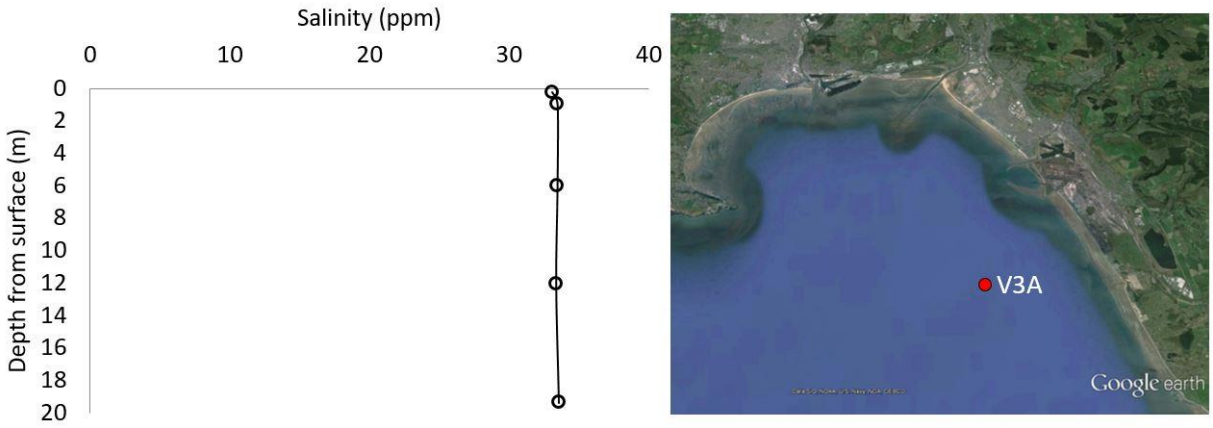

Figure 13: Typical vertical salinity profile in Swansea Bay (location V3A; Ahmadian et al., 2013)

The interaction between suspended sediment levels and FIOs has been studied previously and its importance highlighted (Haung et al., 2015 and 2018, Ahmadian et al., 2010, Yang et al., 2008). Since this study was mainly focused on implementation of the decay rate in the absence of sediment data, sediment modelling was not considered as a part of this study. While surveys have shown variations in suspended sediment concentrations throughout the water column, data are sparse and a constant value of 84.82mg/l was assumed, based on measurements taken nearby at Langland Bay and Porthcawl (Stapleton et al., 2007b). Based on this assumption Equations 4 to 8 are considered a function of light intensity and water depth. The relationship between the T_{90} value and these variables is shown in Figure 14, using Latin hypercube sensitivity analysis (Iman, 2008; Stein, 1987). The water depth, which varied up to the maximum natural (i.e. not dredged)

water depth in Swansea Bay and irradiance varied over the feasible parameter range from the reviewed literature (Stapleton et al., 2007a) and site measurements (Aberystwyth University and University College Dublin, 2018).

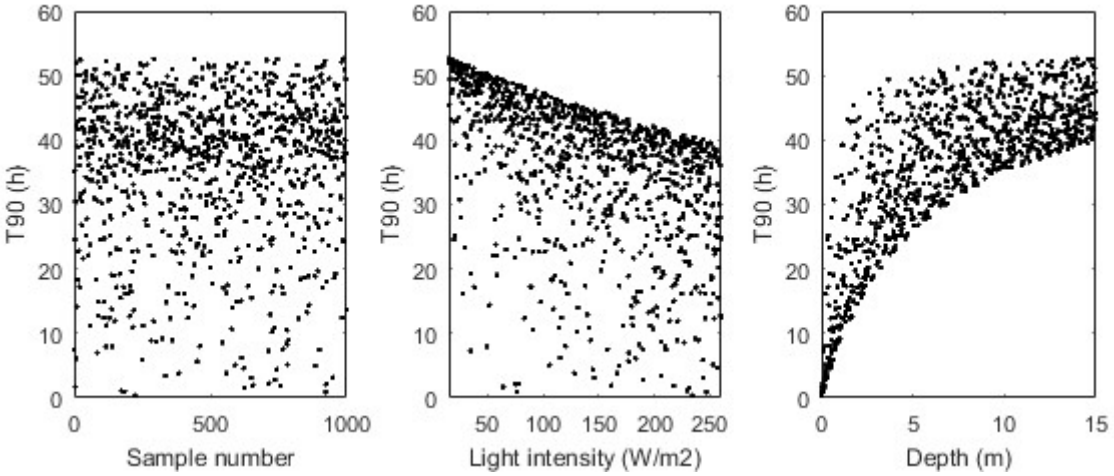

Figure 14: Latin hypercube sensitivity analysis of decay rate based on depth and irradiance variations with suspended solid concentrations, salinity and temperature being considered constant

Data recorded over the 2012 simulation period shows an average daily maximum of 170 W/m^2. This fits within the 0 to 260 W/m^2 range of light intensity reported by Stapleton et al. (2007a). A sine function, covering the range 0 to pi, was used to represent the variation in light intensity over daylight hours (06:00 to 18:00), as proposed by Boye et al. (2015) and as shown in Figure 15. Night-time values were recorded at 0.15 W/m^2. However, a lower limit of 15 W/m^2 was placed on this value to prevent the T_{90} value tending towards infinity as depth and solar intensity approached zero.

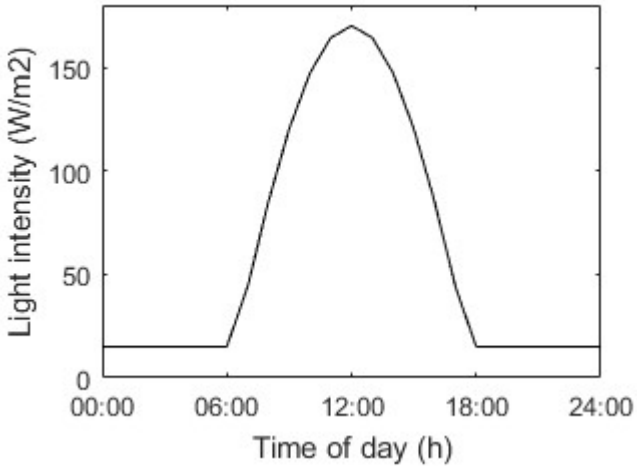

Figure 15: Assumed light intensity function over a typical day

3 Hydrodynamic model validation

A constant Manning's coefficient was used throughout the model domain. Based on the range of suggested roughness values presented in Chow (1959), water levels were calibrated by testing values of 0.02, 0.025 and 0.03 respectively, which were deemed suitable for excavated or dredged channels, and clean, straight main channels. The model was found to have low sensitivity to the bed roughness and a value of 0.025 was selected as that producing the best fit. Calibration and validation of water levels were initially carried out against tide gauge records provided by the British Oceanographic Data Centre (BODC) (https://www.bodc.ac.uk/), at four sites throughout the domain, as shown in Figure 6, over a spring-neap tidal cycle. Two sites, namely Illfracombe and Avonmouth, were used for model calibration and the sites at Mumbles and Hinkley Point were used for model validation. A plot comparing measured and predicted water levels at the Mumbles site, which is located at the Western edge of Swansea Bay, is shown in Figure 16. The Root Mean Square Error (RMSE) and Nash Sutcliffe Efficiency (NSE) (Nash and Sutcliffe, 1970; Coz et al., 2019) values were used to assess the correlation of the predicted and measured data. The RMSE and NSE values for the Mumbles site were 0.31 and 0.99, respectively, which showed good correlation between the measured and predicted data. There is a gap in the BODC data record for this site, which can be seen in Figure 16.

Further validation of water level predictions was carried out using Acoustic Doppler Current Profilers (ADCP), deployed at 5 sites within Swansea Bay (as shown in Figure 17), from 21/07/2012 to 28/08/2012 (Aberystwyth University and University College Dublin, 2018; EMU Limited, 2012) . The survey was carried out using a bed mounted Nortek Aquapro (EMU Limited, 2012). This further validation also confirmed good correlation between the measured and predicted water levels. The velocity magnitudes and directions predicted by the model were validated against the ADCP measurements, which were averaged over depth. The comparisons of the measured and predicted velocity magnitudes and directions showed that model predictions matched the measured data and that the model predictions were reliable. Typical comparisons of measured and predicted velocity magnitudes and directions are shown in Figures 15 and 16. Current direction are presented with respect to due north.

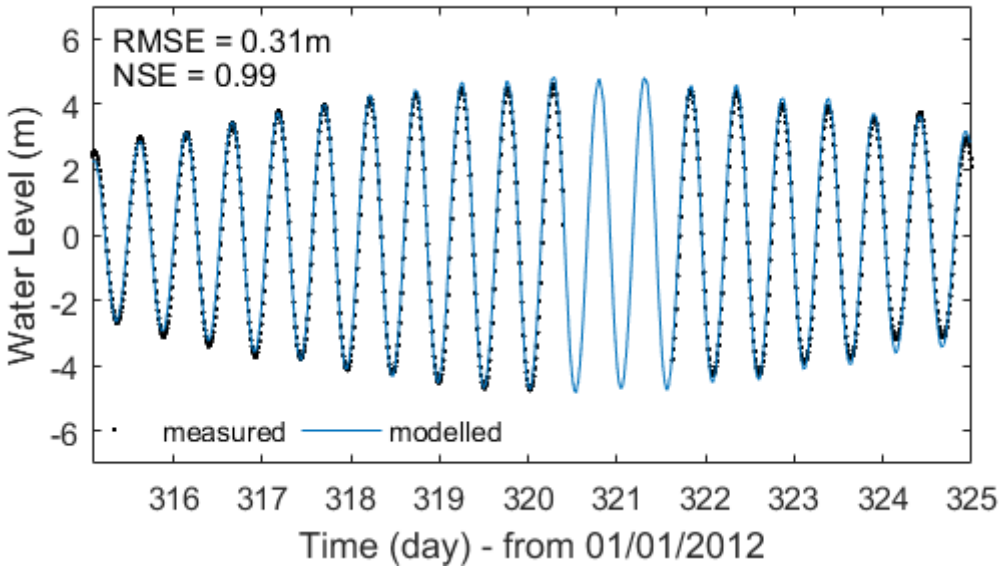

Figure 16: Plot of calibrated water levels measured at Mumbles, adjusted relative to MSL, n = 0.025

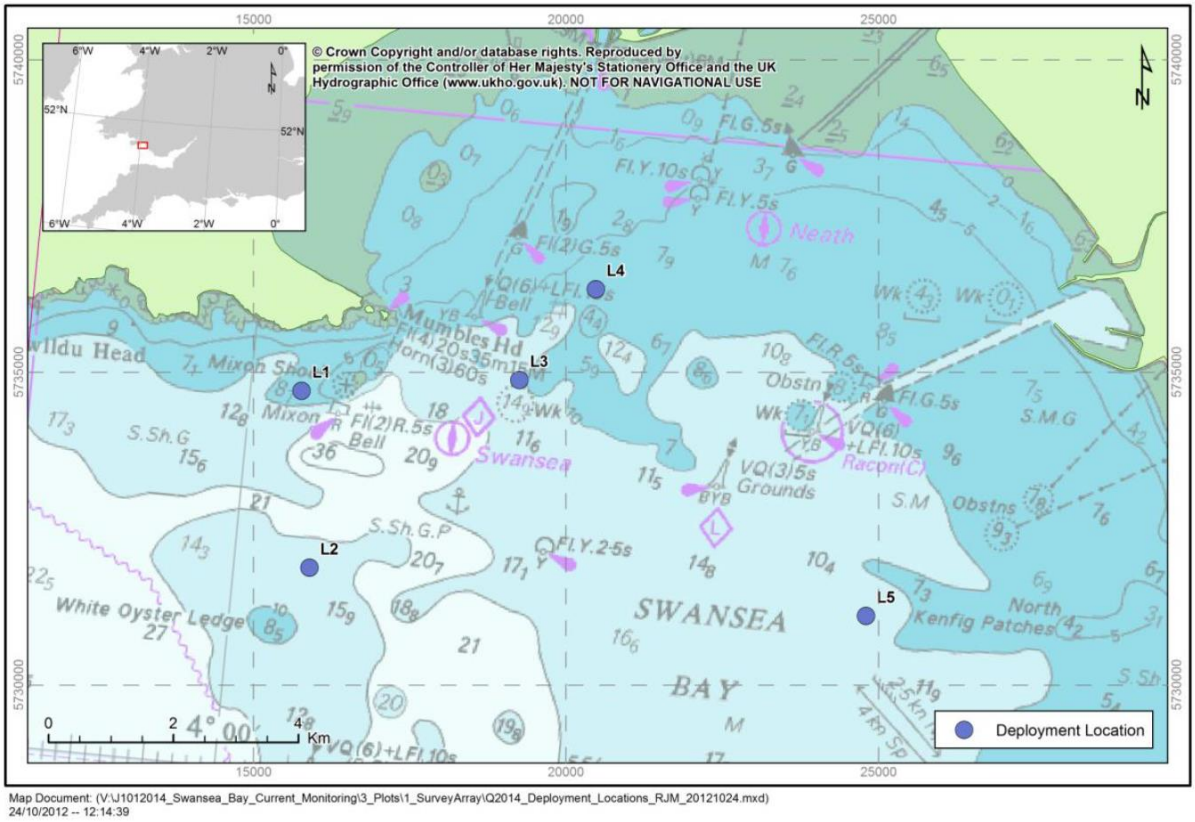

399

400 *Figure 17: ADCP survey locations in Swansea Bay*

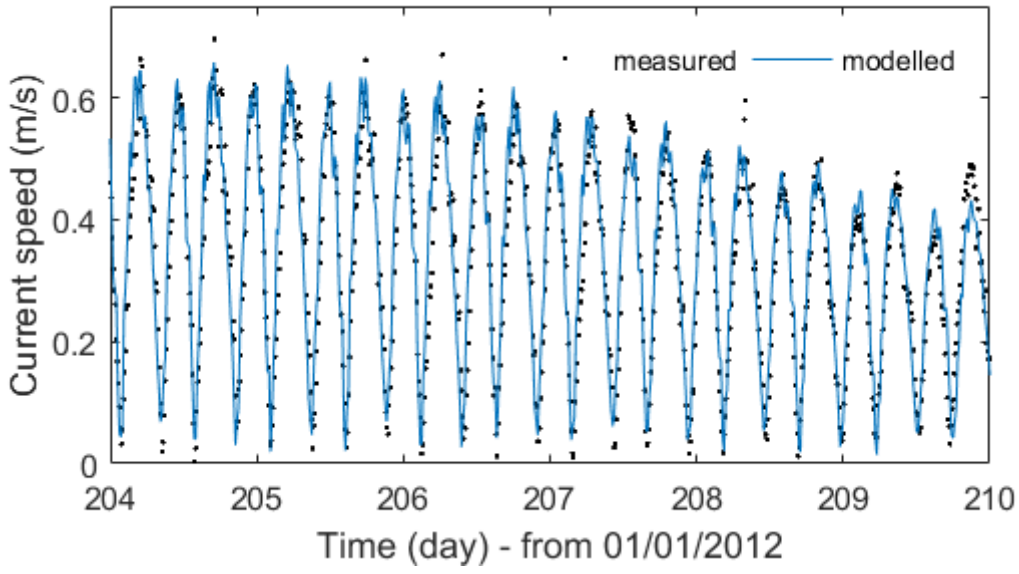

401

402 *Figure 18: Plot of validated current speed in Swansea Bay at location L2*

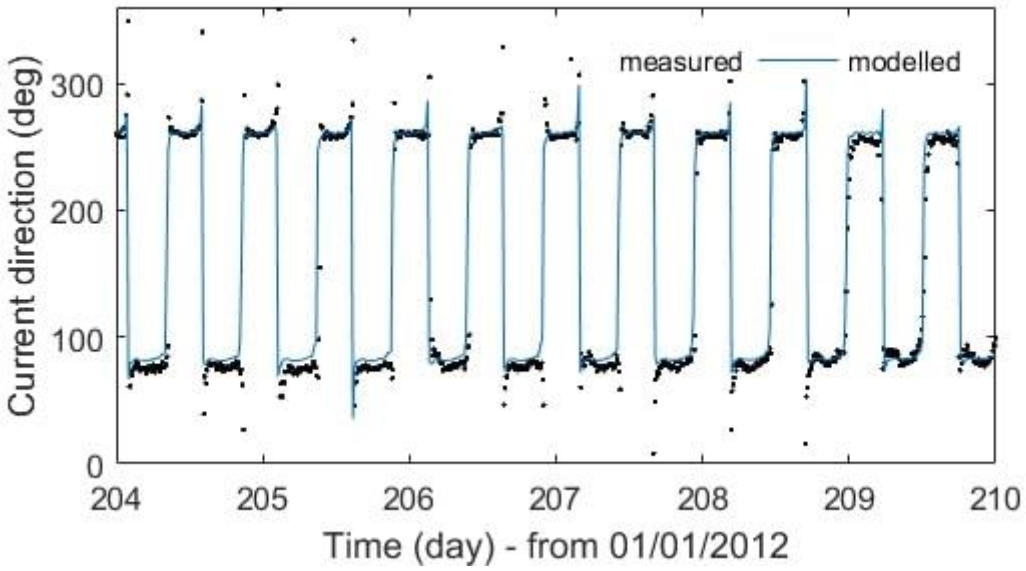

403

404 *Figure 19: Plot of validated current direction in Swansea Bay at location L2*

405 # 4 Results

406 The model performance was next assessed using the *E. coli* records taken on 15th November 2012
407 (Aberystwyth University and University College Dublin, 2018). Monitoring at the Swansea Bay and
408 Aberafan DSPs was done along the transects shown in Figure 1. The measured and predicted
409 values were compared using the new developments discussed in 2.4.1 and 2.4.2, to assess the
410 performance of each method. For supplementary data omitted from this paper for brevity, see
411 King (2019).

412

413 Figure 20 presents a comparison between the 2D and 3D modelled *E. coli* concentration
414 predictions at the Swansea Bay DSP, using stationary point sources and a depth-averaged decay
415 function. To mirror the sampling strategy used in the field the predictions shown are taken at the
416 shallowest transect point greater than or equal to the sampling depth (0.5 m, see Section 2.1 and
417 Figure 2b). Thus, the line plots shown correspond to multiple locations. Note that all 3D results
418 presented herein have been averaged over the vertical layers to provide an indication of the
419 concentration throughout the water column, rather than within a single layer. It can be seen in
420 Figure 20 that the 2D model predicts higher concentrations than the 3D model.

The predicted concentrations using the depth averaged decay function at all points along the DSP transect within the 2D model are plotted in Figure 21, while the concentration plots around the DSP and the monitoring points along the DSP transect are shown in Figure 22. It can be seen in Figure 21 that at any point in time, there are significant spatial differences in the predicted *E. coli* concentrations at each transect point, with a range of up to half the magnitude of the highest predicted concentrations. The point which is considered a best fit to the measured data has been highlighted.

Figure 23 presents a comparison between the measured and predicted *E.coli* concentrations at the Swansea Bay DSP using depth-averaged and varying decay rates. It can be seen that lower concentrations were predicted when using the depth-varying decay function.

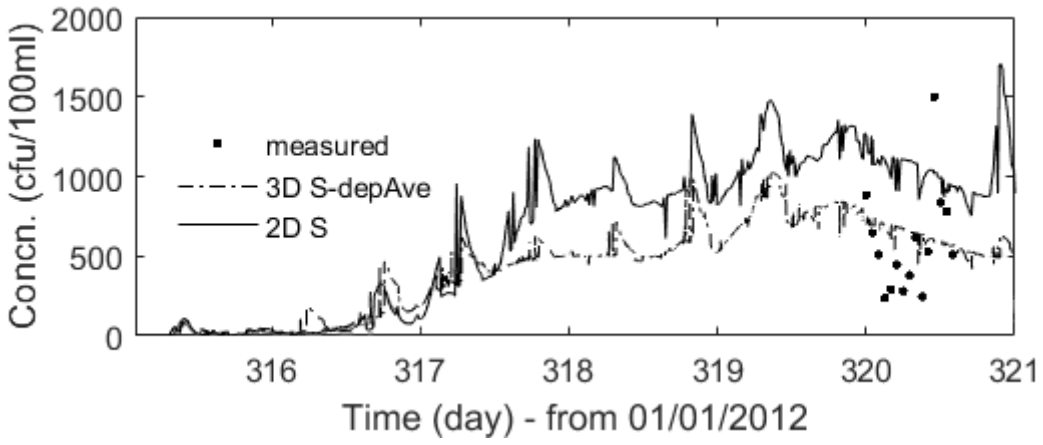

Figure 20: Comparison between the measured and predicted E.coli concentrations at the Swansea Bay DSP, using the Stapleton et al. (2007a) (S) decay function in the 2D and 3D models

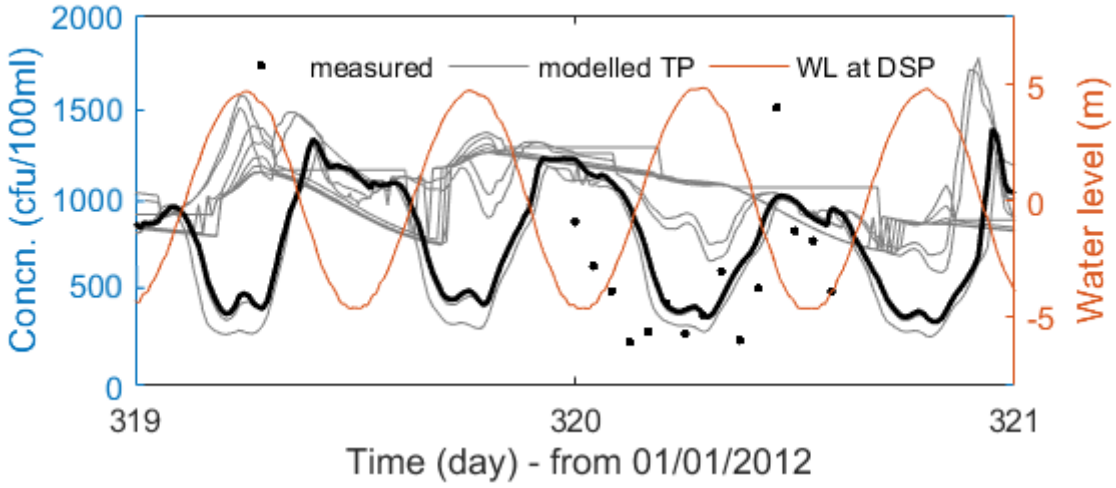

438

439 *Figure 21: Comparison between the measured and predicted E. coli concentrations at each*
440 *monitoring location along the Swansea Bay DSP transect (TP), using the Stapleton et al. (2007a)*
441 *decay function in the 2D model. Plotted alongside the predicted water level at the most offshore*
442 *monitoring location*

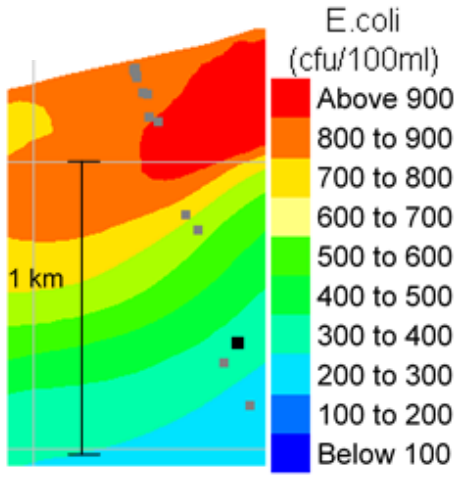

443

444 *Figure 22: Surface plot of the predicted E. coli concentrations along the Swansea Bay DSP transects,*
445 *using the Stapleton et al. (2007a) decay function in the 2D model at 19:11:57 on 15/11/12 (high*
446 *tide)*

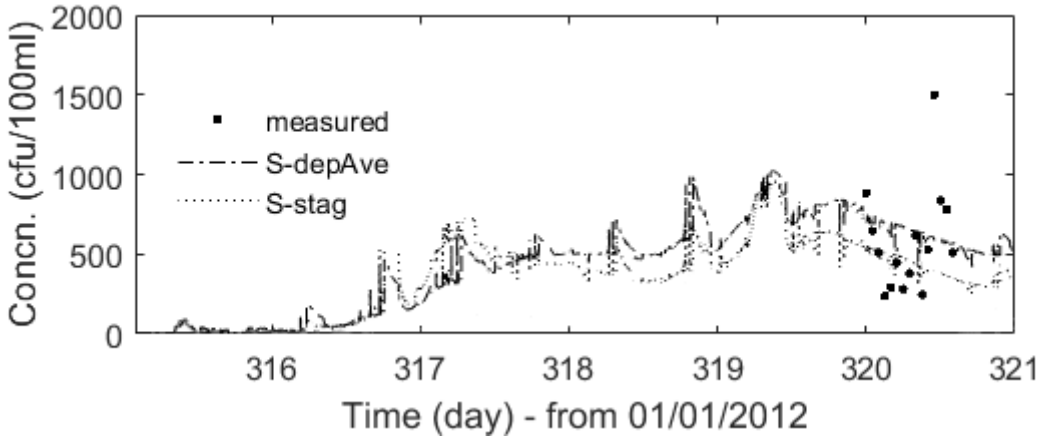

447

448 *Figure 23: Comparison between the measured and predicted E.coli concentrations at the Swansea*
449 *Bay DSP using depth-averaged and varying Stapleton et al. (2007a) (S) decay functions in the 3D*
450 *model*

451 Plots comparing the measured and predicted *E.coli* concentrations at the Swansea Bay DSP using
452 the static and improved source release models are shown in Figures 24 and 25. Figure 24 presents
453 this comparison at the Swansea Bay DSP whereas Figure 25 includes the wider Bay area and
454 highlights the spatial variability in concentration predictions between the methods.

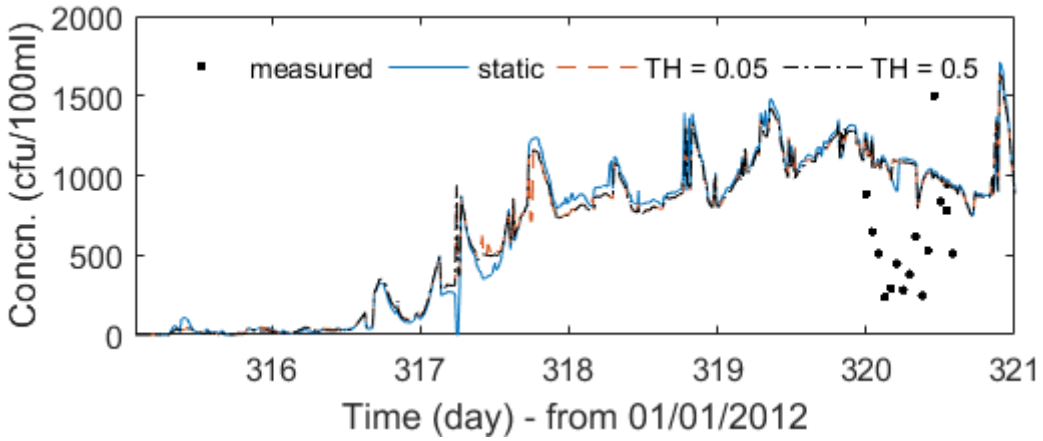

455

456 *Figure 24: Comparison between the predicted E. coli concentrations at the Swansea Bay DSP, using*
457 *static sources, and improved source representation with two threshold depths (TH)*

458

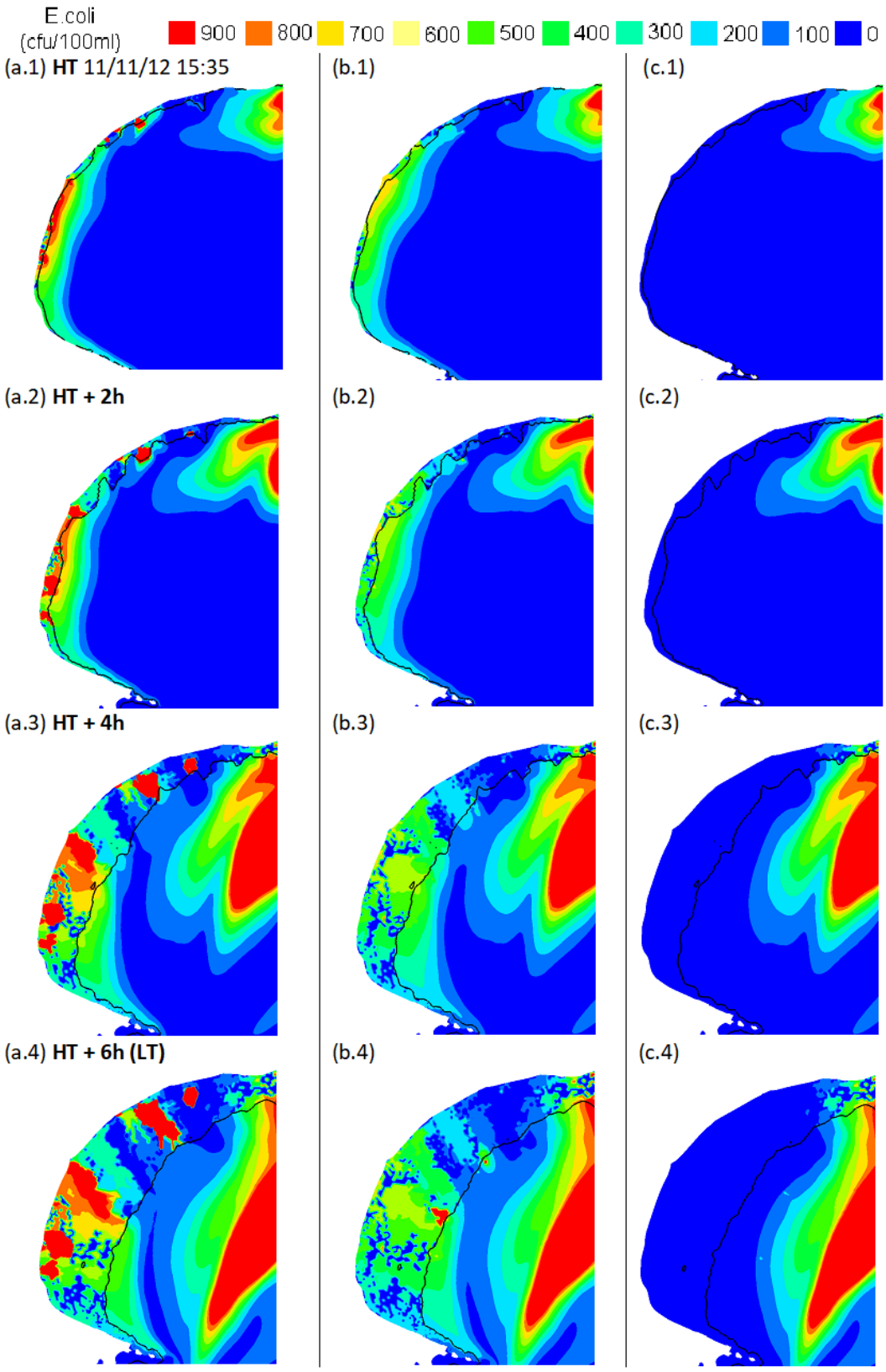

Figure 25: Comparison of the predicted E. coli concentration distributions in Swansea Bay, using the 2D model with static sources, improved source representation (TH = 0.05), and deep water sources; (a), (b) and (c), respectively

5 Discussion

5.1 Comparison of 2D and 3D decay model setup

It can be seen in Figure 20 that the 2D model predicts higher bacterial concentrations than the 3D model. This can be partly attributed to the method used in inclusion of the rivers Tawe and Neath in the 2D model, which were included in the 3D model by accumulating the flow and bacterial input at a single point due to computational time issues, and can be explained by looking at Figures 26 and 27.

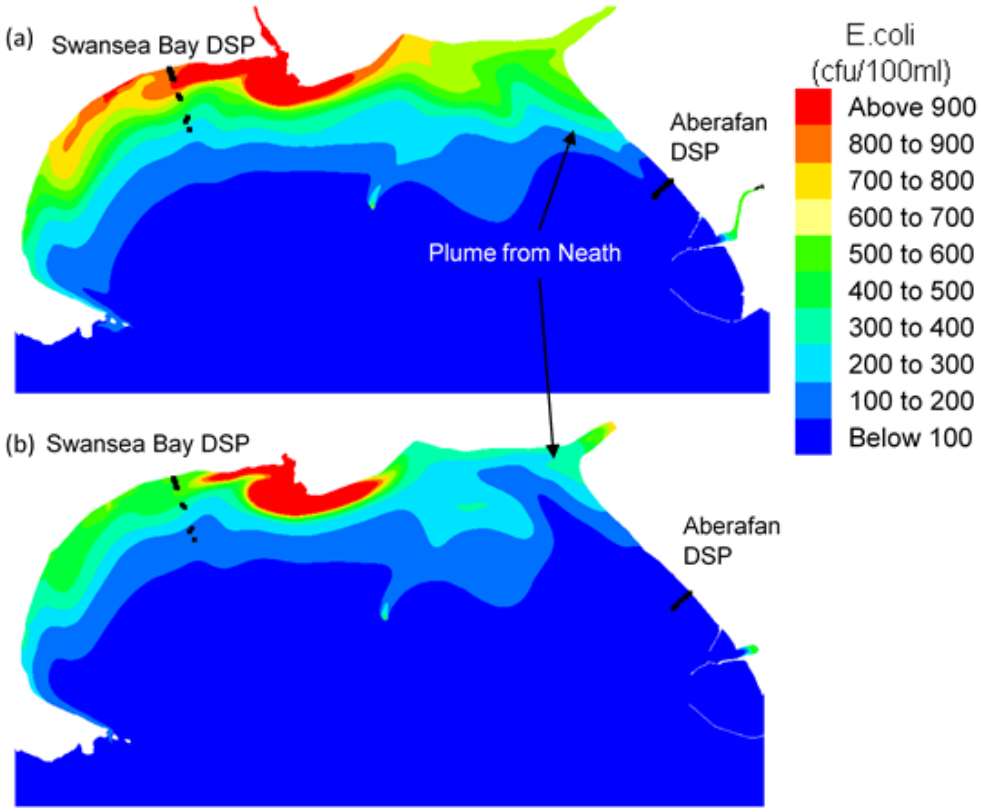

Figure 26: Comparison of the predicted E. coli concentration distribution in Swansea Bay, at 19:16 on 15/11/12 (HT), using the Stapleton et al. (2007a) decay function in the 2D (a) and 3D (b) models. Depth-averaged decay function used in the 3D model

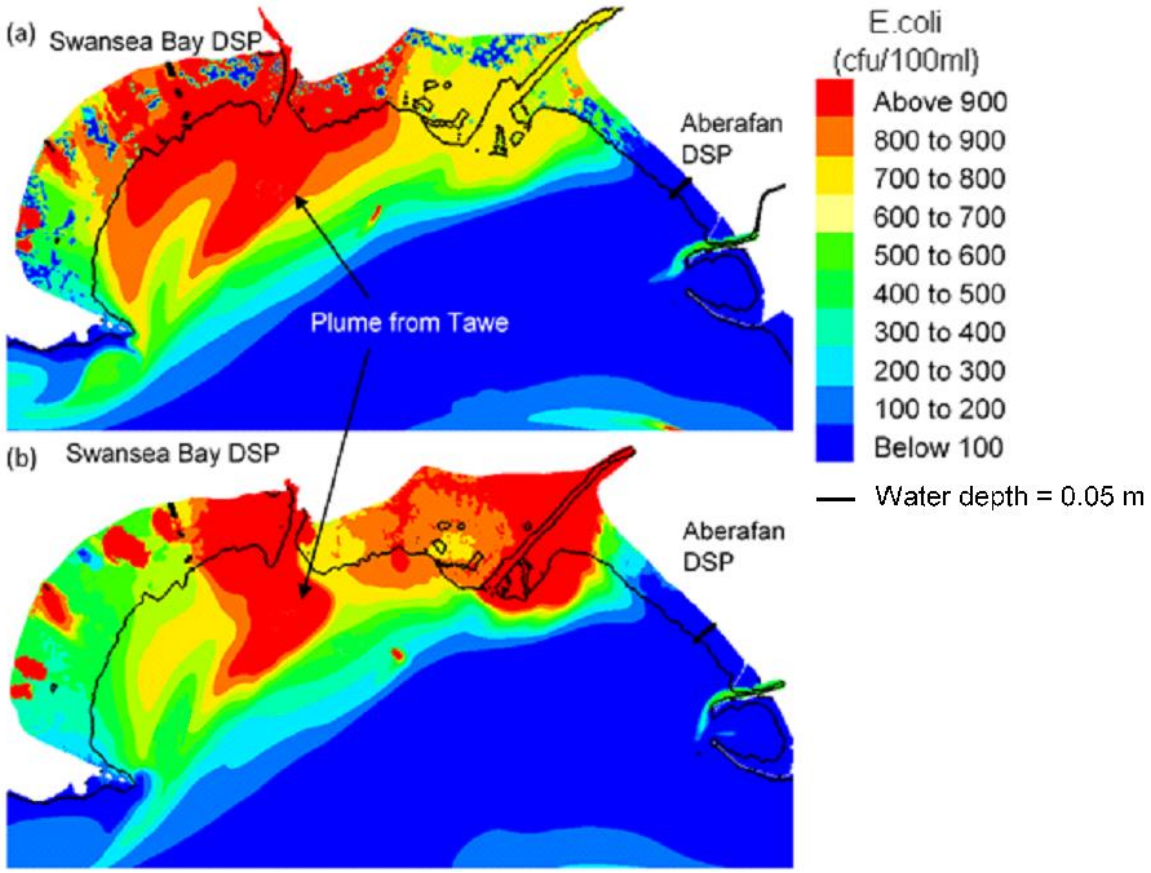

476

477 *Figure 27: Comparison of the predicted E. coli concentration distribution in Swansea Bay, at 12:09*
478 *on 15/11/12 (LT), using the Stapleton et al. (2007a) decay function in the 2D (a) and 3D (b)*
479 *models. Depth-averaged decay function used in the 3D model. The black line represents a water*
480 *depth of 0.05 m.*

481 Based on the location of the model *E. coli* inputs (see Figures 4 and 5), it can be reasoned that the
482 plume from the River Tawe is responsible for the water quality at the Swansea Bay DSP. While this
483 input is included accurately within the 2D model, it is represented as a point source at the river
484 mouth in the 3D model, without an assigned velocity. In this case the flow speed is greatly reduced
485 and the plume does not extend far enough into the Bay during the ebb tide. This highlights the
486 importance of including source term momentum when representing bacterial inputs in 3D models.
487 This may be either by assigning a velocity to point sources or linking 1D river models with the 3D
488 coastal model, with momentum transfer across the linked boundaries.

489

5.2 Spatial and temporal variability

It is suggested that because of the spatial variance in bacterial concentrations shown in Figures 21 and 22, when modelling and sampling it may be prudent to predicted and record FIO levels at multiple locations to ascertain the spatial distribution in bacterial concentration and adequately determinate the risk to bathers. Not doing so may lead to under prediction of this risk and erroneous calibration of the hydro-epidemiological models.

In addition, Figure 21 shows a diurnal pattern in the predicted *E. coli* concentrations at the Swansea Bay DSP. On day 320 this is also seen in the measured data. This diurnal pattern is expected to be due to the accumulative impact of decay during the day following an increase in the solar radiation, as shown in Figure 15. However, other influential factors might be affecting the diurnal pattern, such as a contribution from the sources, tidal dilution or interaction with sediments, and which need to be considered in more detail.

High spatial, and potentially diurnal, variations are seen along all other transects too, thus highlighting the variability of the concentration along a beach and at different times. Therefore, although this highlights a potential limitation of the model to calculate processes which take place at a high spatial resolution, it may also be prudent to consider different methods of classifying bathing water sites based on a non-stationary DSP.

5.3 Depth-varying decay

It can be seen in Figure 23 that lower concentrations were predicted when using the depth-varying decay function. To discuss the reason for this reduction in concentration and highlight the applicability of the depth-averaged decay approach, a simplified vertical 1D case is considered. Equation 15 represents a simplified form of Equation 1, reduced to 1D in the vertical and with zero vertical velocity.

$$\frac{\partial C}{\partial t} = \frac{\partial}{\partial z}\left(\nu_T \frac{\partial C}{\partial z}\right) - kC \qquad 15$$

516

517 In this situation the problem is reduced to one controlled by turbulent and molecular diffusion
518 between the layers and decay. This can be further reduced to Equation 2 by setting the turbulent
519 diffusion term to zero. The analytical solution of Equation 15 is then given in Equation 16:

520

$$C(t) = C_0 e^{-kt} \qquad 16$$

521

522 where C(t) is the concentration at time t, C_0 is the concentration at time t = 0 and k is the decay
523 rate (1/d). For a simple 5-layer problem, with a node spacing of 1 m, we look at the decay of an
524 initial tracer (bacteria) concentration of 1,000 (dimensionless) over 2 days. The equation was
525 solved at a time step of 1 minute using the finite different method, with a first order forward
526 difference scheme in time and a second order central difference scheme in space. The boundary
527 value problem was solved at the surface and bed introducing phantom layers, with a value equal
528 to the adjacent real boundary. Thus, diffusion only acts within the domain. Values for suspended
529 sediment concentration, salinity and temperature were set as those used in the Swansea Bay
530 study, and with the light intensity fixed at 260 W/m^2.

531

532 A comparison of the concentrations over depth predicted by the analytical solution and two
533 different decay approaches used in this study is illustrated in Figure 28. As can be seen there is
534 good agreement between the analytical solution and the finite difference solutions, using a depth-
535 varying decay, when the tracer diffusion term is set to zero. This result confirms the validity of this
536 method. For further information, see King (2019) wherein the data plotted in (a) is presented in
537 tabular form. Comparing the use of the depth-varying and depth-averaged decay functions, it can
538 be seen in (b) that the overall concentration in the water column is less when a depth-varying

approach was used. This is because the exponentially larger decay rate in the surface layers causes a greater reduction in the concentration than that predicted at depth (see Figure 7).

Due to the increased transport of bacteria from regions of high concentration at depth to lower concentrations at the surface, this results in higher concentrations in the surface layers, reduced concentrations at depth and a reduction in total concentration in the water column. Bacteria in the surface layers continues to decay at a faster rate, increasing the concentration gradient and hence the movement of bacteria between layers.

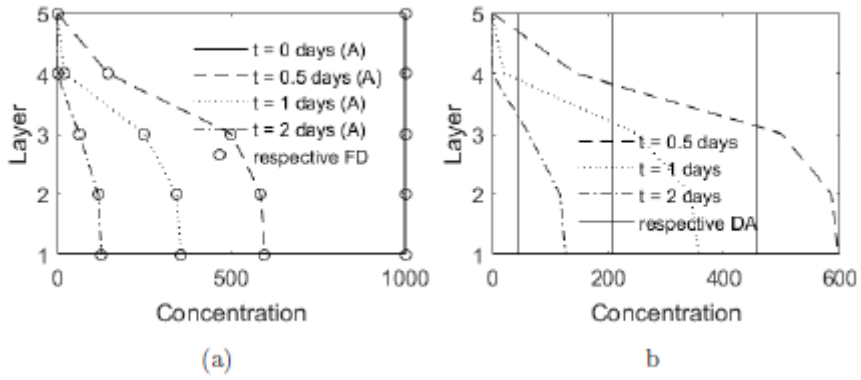

Figure 28: Solution of simplified 5 layer decay problem; (a) comparison between analytical and finite difference (FD) solutions using a depth-varying decay rate, where T = 0; and (b) comparison between FD solutions using depth-averaged (DA) and varying solutions

This interchange between layers will be further increased by including the velocity term in Equation 15, where there is an upward flow such as in Swansea Bay, and in the vicinity of long sea outfall diffusers with a vertical orientation.

5.4 Moving discharge

The following section presents a comparison between the use of static and non-stationary bacterial point inputs in the 2D model of Swansea Bay. In considering the predicted surface concentration distributions (see Figure 25), there are clear differences observed when comparing the two approaches over a tidal cycle. At high tide there are elevated concentrations in the static discharge model and the *E. coli* plume extends a greater distance into the western region of

Swansea Bay. During the ebb tide the differences become more pronounced as the plume spreads over a larger beach area above the water line. In comparison, the predicted concentrations in the improved source model are greatly reduced and the plume below the water line is reduced in size. There are also small regions with high *E. coli* concentrations immediately below the waterline, and in the vicinity of the source points, which have more serious implications on the predicted risk to bathers. Therefore, implementation of the mobile source point could significantly impact the results and should be considered in future studies. With regard to the *E. coli* distribution above the water line, this will have a greater implication if the beach sand is considered as a diffuse bacterial source and sink, in a similar manner to how Abu Bakar et al. (2017b) modelled inter-tidal marshland in the Loughor Estuary, UK. Furthermore, these regions may aid in providing more accurate predictions of the location of 'safe' and 'no go zones', on the beach and in the water, which is of utmost importance when disseminating bathing water information to beach goers, as advised in the rBWD.

As shown in Figure 24, for the majority of the simulation period, use of the improved source model results in lower concentrations. This is due to increased dilution as the tracer is released into deeper water. While it is not possible to discern a difference between the two improved source models using different threshold depths, it can be seen in Figure 25 that if all release locations are moved to a point below the low tide line, *E. coli* concentrations in the nearshore region are under predicted throughout the tidal cycle, due to increased dilution. This indicates that correctly modelling the beach sources is important in order to predict accurately the dynamics governing bacterial transport. It is therefore suggested that the apparent invariance between the static and improved source release models seen in Figure 24 is due to the distance of the DSP from the bacterial beach source locations (see Figure 1), as well as the influence of the River Tawe on the DSP as previously explained.

It can be seen from these results that although using the new model results in minor improvements in *E. coli* concentration predictions at the DSP and within Swansea Bay, the

differences between model predictions are not significant enough to warrant the choice of one method over the other for this case study, or at this stage in model development.

6 Conclusions

Two computational models, one 2D and one 3D, were set up using the TELEMAC suite of models to implement new enhancements in simulating the transport and decay of *E. coli* in a data rich case study site. The models and the data were then compared for a range of different modelling approaches. The case study site was Swansea Bay, located in South West of the UK, where over 7,000 samples were taken during 2011. The 3D model was found to under predict bacterial concentrations due to the inclusion of the Rivers Neath and Tawe as point sources, and without momentum conservation. The application of a 3D model in a well-mixed marine environment, where a 2D depth averaged approach is usually adopted, highlights the impact of a vertically variable decay through the water column. Application of this method is an important step in improving the reliability of 3D deterministic epidemiological models, to ensure that decay processes are represented realistically. Of the two methods used to calculate decay throughout the water column in the 3D model, namely depth-varying and depth-averaged, the depth-varying approach was found to predict lower bacterial concentrations due to the exponential decrease in light intensity with depth and the associated effect on the decay rate. It is therefore suggested that in 3D modelling studies a depth-varying decay model should be used as it provides a more accurate representation of the vertical spatial variation in bacterial die-off rates. Using the 2D model, an improved method of representing beach sources was developed to mimic the streams discharging along the Swansea Bay beach. Rather than being considered stationary, the sources were moved along a transect throughout the simulation period, to ensure they discharged just below the waterline. This provided more accurate predictions of the spatial distribution of *E. coli* within the domain, with the most significant effects noticed above and near the waterline, such as zones of elevated bacterial concentration where the beach streams enter the water. In addition, it highlights the limitations of using TELEMAC to model static beach sources on shallow gradient

beaches, subject to wetting and drying throughout the tidal cycle. Spatial and diurnal variations in bacterial concentrations were seen along the Swansea Bay Designated Sampling Point transect, highlighting the variability of water quality along the beach and at different times. Therefore, it is suggested that bathing water monitoring based on a stationary Designated Sampling Point may lead to incorrect classification of the bathing water quality and provide a false indication of the risk of infection. In addition, it highlights a potential limitation of bacterial models to calculate processes accurately, which take place at a high spatial resolution.

Acknowledgements

This work was supported by the Engineering and Physical Sciences Research Council (grant EP/L016214/1), and the EERES4WATER project, which is co-financed by the Interreg Atlantic Area Programme through the European Regional Development Fund (grant EAPA 1058/2018), which is gratefully acknowledged. The authors are also grateful for the support and data provided by staff at the Centre for Research into Environment and Health (CREH) at Aberystwyth University (particularly Prof. D. Kay and Dr M. Wyer), Natural Resources Wales, and Swansea City County Council and Dwr Cymru. The authors would also like to thank High Performance Computing Wales (HPCW) and Advanced Research Computing at Cardiff (ARCCA) for use of their facilities. The UK coastline shapefile used to create Figure 1 was provided by the OpenStreetMap project (http://openstreetmapdata.com).

References

Aberystwyth University and University College Dublin, 2018. Smart Coasts [online]. Available from: http://smartcoasts.eu/ [accessed 18 August 2018].

Abu Bakar, A., Ahmadian, R. and Falconer. R.A., 2017a. Modelling the transport and decay processes of microbial tracers released in a macro-tidal estuary. Water Research. 123, October, 802-824.

637 Abu Bakar, A., Ahmadian, R. and Falconer. R.A., 2017b. Diffuse bacteria loading from intertidal
638 marshland and impacts to adjacent estuarine water quality. Proceedings of the 37th IAHR
639 World Congress, pp. 3563-3570.

640 Ahmadian, R., Falconer, R. A. and Lin, B., 2010. Hydro-environmental modeling of the proposed
641 Severn barrage. Proceedings of the Institution of Civil Engineers Energy 163(3), pp. 107-117.
642 https://doi.org/10.1680/ener.2010.163.3.107.

643 Ahmadian, R., Bomminayuni, S., Falconer. R.A. and Stoesser, T., 2013. SSC Numerical modelling of
644 flow and faecal indicator organism transport at Swansea Bay, UK. Technical Report.

645 Ahmadian, R., Olbert, A.I., Hartnett, M. and Falconer, R.A., 2014. Sea level rise in the Severn Estuary
646 and Bristol Channel and impacts of a Severn Barrage. Computers & Geosciences, 66, pp. 94-105.

647 Alkan, U., Elliott, D. J. and Evison, L. M. 1995. Survival of enteric bacteria in relation to simulated
648 solar radiation and other environmental factors in marine waters. Water Research, 29(9), pp.
649 2071-2080. https://doi.org/10.1016/0043-1354(95)00021-C.

650 BBC, 2017. UK attracting record numbers of tourists [online]. Available from:
651 https://www.bbc.co.uk/news/business-41564655 [accessed 3 December 2018].

652 Bedri, Z., Bruen, M., Dowley, A. and Masterson, B., 2013. Environmental consequences of a power
653 plant shutdown: A three-dimensional water quality model of Dublin Bay. Marine Pollution
654 Bulletin, 71(1-2), pp. 117–128. https://doi.org/10.1016/j.marpolbul.2013.03.025.

655 Bedri, Z., Corkery, A., O'Sullivan, J. J., Alvarez, M. X., Erichsen, A. C., Deering, L. A., Demeter, K.,
656 O'Hare, G. M. P., Meijer, W. G. and Masterson, B., 2014. An integrated catchment-coastal
657 modelling system for real-time water quality forecasts. Environmental Modelling and Software,
658 61, pp. 458–476. http://dx.doi.org/10.1016/j.envsoft.2014. 02.006.

659 Bedri, Z., O'Sullivan, J. J., Deering, L. A., Demeter, K., Masterson, B., Meijer, W. G., and Hare. G. O.,
660 2015. Assessing the water quality response to an alternative sewage disposal strategy at

661 bathing sites on the east coast of Ireland. Marine Pollution Bulletin, 91(1), pp. 330–346.
662 http://dx.doi.org/10.1016/j.marpolbul.2014.11.008.

663 Bedri, Z., Corkery, A., O'Sullivan, J. J., Deering, L. A., Demeter, K., Meijer, W. G., Masterson, B., 2016.
664 Evaluating a microbial water quality prediction model for beach management under the
665 revised EU Bathing Water Directive. Journal of Environmental Management, 167, pp. 49–58.
666 https://doi.org/10.1016/j.jenvman.2015.10.046.

667 Bomminayuni. S., 2015. Modelling tidal ow for assessment of hydro-kinetic energy and bathing
668 water quality in coastal waters. PhD thesis.

669 Boye, B. A., Falconer. R.A., and Akande. K., 2015. Integrated water quality modelling: Application
670 to the Ribble Basin, U.K. Journal of Hydro-environment Research, 9(2), pp. 187-199.
671 https://doi.org/10.1016/ j.jher.2014.07.002.

672 Chapra. S. C., 1997. Surface Water-Quality Modeling. Mc-Graw Hill, Singapore.

673 Bussi, G., Whitehead, P. G., Thomas, A. R.C., Masante, D., Jones, L., Cosby, J.B., Emmett, B. A., Malham,
674 S. K., Prudhomme, C., Prosser, H., 2017. Climate and land-use change impact on faecal indicator
675 bacteria in a temperate maritime catchment (the River Conwy, Wales). Journal of Hydrology.
676 https://doi.org/10.1016/j.jhydrol.2017.08.011.

677 Chen, W. B. and Liu, W. C., 2017. Investigating the fate and transport of fecal coliform
678 contamination in a tidal estuarine system using a three-dimensional model. Marine Pollution
679 Bulletin, 116(1-2), pp. 365–384. https://doi.org/10.1016/j.marpolbul.2017.01.031.

680 Chow, V. T. 1959. Open-channel hydraulics. McGraw-Hill Book Company, New York.

681 Což, N., Ahmadian, R., Falconer, R.A., 2019. Implementation of a full momentum conservative
682 approach in modelling flow through tidal structures. Water, 11(9), 1917.
683 https://doi.org/10.3390/w11091917.

de Brauwere, A., de Brye, B., Servais, P., Passerat, J. Deleersnijder, and E., 2011. Modelling Escherichia coli concentrations in the tidal Scheldt river and estuary. Water Research, 45(9), pp. 2724–2738. https://doi.org/10.1016/j.watres.2011.02.003.

DHI, 2017a. Bathing Water Quality Forecast at Your Fingertips [online]. Available from: https://www. dhigroup.com/global/news/2017a/02/bathing-water-quality-forecast-at-your-fingertips.

DHI, 2017b. Water Forecast [online]. Available from: http://www.waterforecast.com/.

Droste, R. L., 1997. Theory and Practice of Water and Wastewater Treatment. John Wiley & Sons, Inc, New York.

EMU Limited, 2012. Swansea Bay Current Monitoring Operational Report. Technical report.

European Environment Agency, 2005. Bathing Water Quality [online]. Technical report. Available at: http://www.eea.europa.eu/data-and-maps/indicators/bathing-water-quality [accessed 27 January 2016].

European Parliament, 2006. Directive 2006/7/EC of the European Parliament and of the Council of 15 February 2006 concerning the management of bathing water quality and repealing Directive 76/160/EEC. Official Journal of the European Union, L 064/37.

Feng, Z., Reniers, A., Haus, B. K., Solo-Gabriele, H. M., Wang, J. D., and Fleming, L. E., 2015. A predictive model for microbial counts on beaches where intertidal sand is the primary source. Marine Pollution Bulletin, 94(1-2), pp. 37–47. https://doi.org/10.1016/j.marpolbul.2015.03.019.

DeFlorio-Barker, S., Wing, C., Jones, R. M. and Dorevitch. S., 2018. Estimate of incidence and cost of recreational waterborne illness on United States surface waters. Environmental Health: A Global Access Science Source, 17(1):3. https://doi.org/10.1186/s12940-017-0347-9.

Given,, S., Pendleton, L. H., and Boehm, A. B., 2006. Regional public health cost estimates of contaminated coastal waters: A case study of gastroenteritis at southern California beaches.

708 Environmental Science and Technology, 40(16), pp. 4851-4858.
709 https://doi.org/10.1021/es060679s.

710 Galland, J. C., Goutal, N., and Hervouet. J. M., 1991. TELEMAC: A new numerical model for solving
711 shallow water equations. Advances in Water Resources, 14 (3), pp. 138-148.
712 https://doi.org/10.1016/0309-1708(91)90006-A.

713 Guo, B., Ahmadian, R., Evans, P., Falconer, R.A. (2020). "Studying the Wake of an Island in a
714 Macro-Tidal Estuary." Water (2020) 12, 1225.

715 J. F. Guillaud, A. Derrien, M. Gourmelon, and M. Pommepuy. T90 as a tool for engineers: Interest
716 and limits. Water Sciences and Technology, 35(11-12):277–281, 1997.

717 Lea, W., 1996. Bathing water quality. Science and Environment Section. House of Commons
718 Library, 96/45.

719 J.-M. Hervouet. Hydrodynamics of Free Surface Flows: Modelling with the Finite Element Method.
720 Wiley, Chichester, 2007. URL http://eu.wiley.com/WileyCDA/WileyTitle/productCd-
721 0470035587.html.

722 Huang, G., Falconer, R. A. and Lin, B. 2015. Integrated river and Coastal flow, sediment and
723 Escherichia coli modelling for bathing water quality. Water 7(9), pp. 4752-4777.
724 (10.3390/w7094752)

725 Huang, G., Falconer. R.A. and Lin, B., 2018. Evaluation of E.coli losses in a tidal river network
726 using a refined 1-D numerical model. Environmental Modelling & Software.
727 https://doi.org/10.1016/j.envsoft.2018.07.009.

728 Iman, R. L., 2008. Latin Hypercube Sampling. Encyclopedia of Quantitative Risk Analysis and
729 Assessment. John Wiley & Sons, Ltd. https://doi.org/10.1002/9780470061596.risk0299.

730 King, J., 2019. Investigation and prediction of pollution in coastal and estuarine waters, using
731 experimental and numerical methods. PhD Thesis, Cardiff University, Cardiff.

Kopmann, R. and Markofsky, M., 2000. Three-dimensional water quality modelling with TELEMAC-3D. Hydrological Processes, 14(13), pp. 2279–2292, https://doi.org/10.1002/1099-1085(200009)14:13h2279:: AID-HYP28i3.0.CO;2-7.

Mancini, J. L., 1978. Numerical Estimates of Coliform Mortality Rates under Various Conditions. Water Pollution Control Federation, 50(11), pp. 2477–2484.

Mattioli, M. C., Sassoubre, L. M., Russell, T. L, and Boehm, A. B., 2017. Decay of sewage-sourced microbial source tracking markers and fecal indicator bacteria in marine waters. Water Research, 108, pp. 106– 114. https://doi.org/10.1016/j. watres.2016.10.066.

Nash J. E. and Sutcliffe, J. V., 1970. River Flow Forecasting Through Conceptual Models Part I-a Discussion of Principles. J. Hydrology, 10(3), pp. 282–290. https://doi.org/10.1016/0022-1694(70)90255-6.

Scottish Government, 2018. Value of bathing waters and influence of bathing water quality: Technical research report. Technical report. https://www.gov.scot/publications/. Accessed: 2018-12-03.

Stapleton, C. M., Wyer, M. D., Kay, D., Bradford, M., Humphrey, N., Wilkinson, J., Lin, B., Yang, L., Falconer. R.A. , Watkins, J., Francis, C. A., Crowther, J., Paul, N. D., Jones, K., and McDonald, A. T., 2007a. Fate and transport of particles in estuaries - Volume IV: Numerical modelling for bathing water enterococci estimation in the Severn estuary. Technical report, Environment Agency, Bristol. Technical report.

Stapleton, C. M., Wyer, M. D., Kay, D., Bradford, M., Humphrey, N., Wilkinson, J., Lin, B., Yang, L., Falconer. R.A. , Watkins, J., Francis, C. A., Crowther, J., Paul, N. D., Jones, K., and McDonald, A. T., 2007b. Fate and transport of particles in estuaries - Volume III : Laboratory experiments , enterococci decay rates and association with sediments. Environment Agency, Bristol. Technical report.

Stein, M., 1987. Large Sample Properties of Simulations Using Latin Hypercube Sampling. Technometrics, 29(2), pp.143-151.

758 The University of Edinburgh, 2016a. EDINA Marine Digimap Service [online]. Available from:
759 https://digimap.edina.ac.uk/ [accessed: 1 September 2016].

760 The University of Edinburgh, 2016b. 1 Arcsecond Gridded Bathymetry (ASC geospatial data)
761 [online]. Available from: http://digimap.edina.ac.uk [accessed 1 September 2016].

762 Thomann, R. V., and Mueller, J. A., 1987. Principles of Surface Water Quality Modeling and Control.
763 HarperCollins, New York.

764 Visit Britain, 2017. GB Tourism Survey: 2017 overview [online]. Available from:
765 https://www.visitbritain.org/gb-tourism-survey-2017-overview [accessed 3 December
766 2018].

767 Weiskerger, C. J. and Phanikumar, M. S., 2020. Numerical Modeling of Microbial Fate and Transport
768 in Natural Waters: Review and Implications for Normal and Extreme Storm Events. Water,
769 12(7), 1876.

770 White, E., Saunders, A., Gibson, J., and Barcock, N., 2014. Tidal Lagoon Swansea Bay Marine Water
771 Quality Assessment. Supporting Technical Information. Tidal Lagoon Swansea Bay Limited.
772 Technical report.

773 World Health Organization, 2003. Guidelines for safe recreational water environments. Volume 1,
774 Coastal and fresh waters. World Health Organization.
775 https://apps.who.int/iris/handle/10665/42591.

776 Xu, P., Brissaud, F., and Fazio, A., 2002. Non-steady-state modelling of faecal coliform removal in
777 deep tertiary lagoons. Water Research, 36(12), pp. 3074–3082.
778 https://doi.org/10.1016/S0043-1354(01) 00534-6.

779 Yang, L., Lin, B. and Falconer, R. A, 2008. Modelling enteric bacteria level in coastal and estuarine
780 waters. Proceedings of the Institution of Civil Engineers Engineering and Computational
781 Mechanics 161(4), pp. 179-186.